J Mater Sci: Mater Electron **(2026) 37:560**

Waste-derived hydroxyapatite reinforced piezoelectric geopolymer hybrid composite for sustainable energy-harvesting applications

Arun Murugesan[1], Nidhya Rathinavel[1], Karthick Jaisankar[1], Balaji Ravi[1], and Natrayan Lakshmaiya[2,*]

[1] *Department of Civil Engineering, PSG Institute of Technology and Applied Research, Neelambur, Coimbatore 641062, India*
[2] *Department of Research and Innovation, Saveetha School of Engineering, SIMATS, Chennai, Tamil Nadu 602105, India*

Received: 25 November 2025
Accepted: 9 March 2026
Published online: 14 March 2026

ABSTRACT

Traditional piezoelectric materials are expensive and environmentally unsustainable, limiting their adoption in energy-harvesting building applications. This study proposes an eco-friendly approach for developing a waste-derived hydroxyapatite (HAP)-reinforced piezoelectric geopolymer hybrid composite using eggshell waste and fly ash. Eggshell-derived calcium carbonate was converted into hydroxyapatite through a controlled precipitation process, and the synthesized HAP was characterized for structural purity, morphology, and dielectric properties. Geopolymer composite specimens of 50 mm cubic geometry were fabricated by incorporating 15 wt% HAP, 25 wt% ZnO, and 10 wt% TiO_2 into a Class F fly ash-based geopolymer matrix and cured at 70 °C for 48 h. Under uniaxial compressive loading, the hybrid composite generated a maximum piezoelectric voltage output of 0.149 V at a compressive stress of 22.12 MPa, while maintaining a compressive strength suitable for non-structural construction applications. Microstructural analysis confirmed uniform dispersion of HAP within the geopolymer matrix, contributing to enhanced interfacial polarization and dielectric response. The results demonstrate that waste-derived HAP can function as an effective, lead-free piezoelectric phase, enabling the development of sustainable, energy-responsive geopolymer materials for self-sensing and energy-harvesting applications.

1 Introduction

The global construction industry faces increasing pressure to mitigate its environmental footprint while maintaining structural performance. Ordinary Portland cement (OPC), the dominant binder in construction, is responsible for nearly 8–10% of global CO_2 emissions due to its energy-intensive clinkerization process and limestone calcination [1–3]. To achieve carbon neutrality, the development of sustainable, multifunctional alternatives to OPC has become imperative [4–6]. Geopolymer binders, synthesized through the alkaline activation of aluminosilicate rich by-products such as fly ash, slag, or metakaolin, have emerged as a

Address correspondence to E-mail: natrayanphd@gmail.com

viable substitute. These binders exhibit high compressive strength, chemical stability, and up to 80% lower CO_2 emissions than OPC. Beyond sustainability, geopolymers serve as adaptable matrices for incorporating functional materials, enabling smart features such as self-sensing and energy harvesting [7–10].

Among these functionalities, piezoelectricity, the ability to generate electrical energy from mechanical stress, offers unique opportunities for self-powered sensing and energy-harvesting infrastructure [11, 12]. Embedding piezoelectric phases within geopolymer matrices can transform passive structural components into active systems capable of monitoring stress, vibration, or damage in real time. However, conventional piezoelectric ceramics such as lead zirconate titanate (PZT) contain toxic lead and require high sintering temperatures, conflicting with environmental and sustainability objectives [13–15].

Hydroxyapatite (HAP), a calcium phosphate compound ($Ca_{10}(PO_4)_6(OH)_2$), has emerged as a promising, lead-free alternative. HAP possesses a non-centrosymmetric hexagonal crystal structure that enables moderate piezoelectric response, along with excellent biocompatibility and chemical stability [16, 17]. While traditionally used in biomedical applications, recent studies suggest its potential as a functional piezoelectric phase for composite materials. Importantly, HAP can be synthesized from low-cost, renewable precursors, making it attractive for sustainable engineering applications [17].

Specifically, eco-efficient method for HAP synthesis involves the valorization of eggshell waste, a calcium rich by-product of the food industry. Globally, millions of tons of eggshells are discarded annually, creating disposal and environmental challenges [6, 18–22]. Since eggshells consist primarily of calcium carbonate ($CaCO_3$), they can be thermally converted to calcium oxide (CaO) and subsequently reacted with phosphoric acid to produce high-purity HAP. This conversion not only reduces waste and landfill burden but also aligns with circular-economy and low-energy manufacturing principles [23, 24].

Despite its sustainability advantages, the integration of waste-derived HAP into geopolymer matrices remains underexplored, particularly regarding its impact on piezoelectric behaviour. The hydroxyl rich geopolymer network offers favourable interfacial bonding with HAP, potentially enhancing dielectric and electromechanical performance. Additionally, incorporating semiconducting oxides such as zinc oxide (ZnO) and titanium dioxide (TiO_2) can create synergistic effects that improve charge mobility and polarization within the hybrid composite.

This study aims to synthesize hydroxyapatite from eggshell waste and evaluate its performance as a piezoelectric additive in fly ash, based geopolymer composites. The work investigates structural, dielectric, and electromechanical properties of hybrid systems containing HAP, ZnO, and TiO_2 nanoparticles. Comprehensive characterization using X-ray diffraction (XRD), scanning electron microscopy (SEM), and energy-dispersive spectroscopy (EDS) was conducted to confirm phase formation, morphology, and interfacial bonding. By integrating waste valorization, sustainable geopolymer chemistry, and functional material design, this research contributes to developing eco-efficient, energy-responsive construction materials. The outcomes demonstrate a pathway toward self-sensing and energy-harvesting infrastructure that advances both environmental sustainability and material innovation.

2 Research gap and novelty

Previous research has examined piezoelectric fillers in cement and geopolymer matrices, yet there has been minimal research on using waste-derived hydroxyapatite as a multifunctional additive. The research still lacks understanding about how eggshell-derived HAP and ZnO and TiO_2 nanoparticles interact to produce electromechanical coupling effects in geopolymer systems.

The present study addresses these gaps by developing a low-temperature, lead-free, waste-derived hybrid composite and systematically investigating its structural, dielectric, and piezoelectric performance. The research introduces an innovative method that combines biogenic calcium materials with geopolymer binders to create sustainable energy-harvesting capabilities.

3 Materials and methods

The experimental program for the geopolymer-piezoelectric composite consists of the principles of piezoelectric generation, raw material selection, HAP characterisation, and geopolymer-piezoelectric composite performance evaluation under mechanical stress.

3.1 Principles of piezoelectric generation

The piezoelectric property of the geopolymer composite, is mainly due to HAP non-centrosymmetric crystal lattice and the semiconducting properties of ZnO and TiO_2. The application of mechanical stress causes the deformation of the lattice, which in turn induces the alignment of dipoles and the creation of potential differences between the electrodes. Figure 1, illustrates the piezoelectric generation, while the composite is subjected to mechanical stress. The polarizations within the geopolymer matrix get greater because of the interfacial charge accumulation at HAP gel boundaries. The presence of ZnO nanoparticles, which are the electron-donating centers, is improving the mobility of charges, whilst TiO_2 is providing the dielectric stability. This combination is creating a micro-capacitive network that is storing and releasing charges in the process of loading and unloading cycles.

The natural flexibility of the geopolymeric binder helps in the transfer of external stresses to the piezoelectric phases that are embedded, thus ensuring a proper electromechanical coupling.

3.2 Raw materials

Eggshell powder was sourced from home food scraps, rinsed thoroughly with distilled water, and then dried

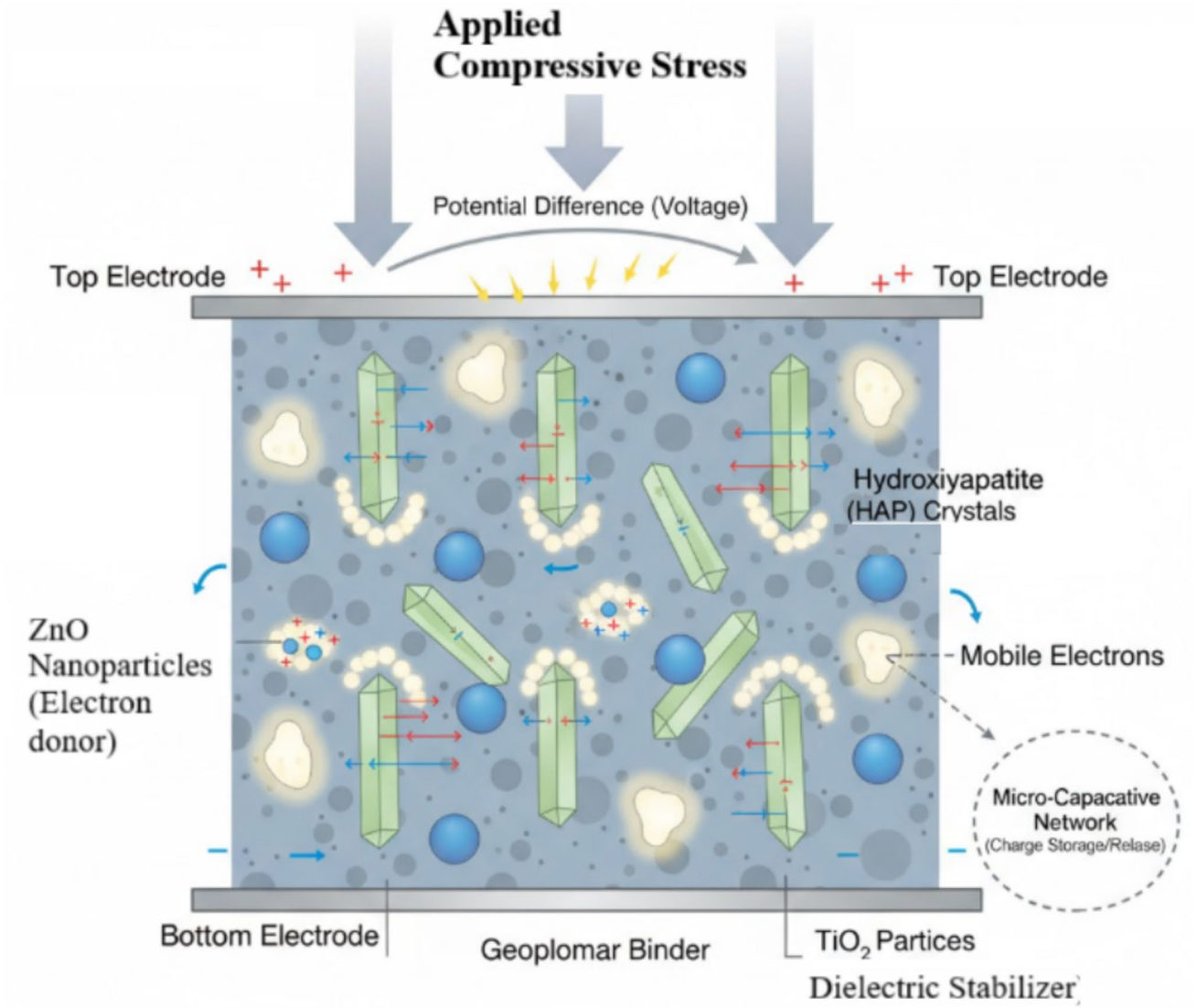

Fig. 1 Principles of piezoelectric mechanism in geopolymer composite

at 105 °C for 12 h to get rid of organic matter and moisture. The shells were then manually broken into small pieces and after drying they are ground to a fine powder (< 100 µm). Phosphoric acid (H_3PO_4, 85%) was the phosphate source for the hydroxyapatite synthesis, while sodium hydroxide (NaOH) was used to control the pH during precipitation. Throughout all reactions, distilled water was used to prevent ionic contamination. Fly ash, which was used as the aluminosilicate precursor for geopolymerization, procured from a thermal power station and was categorized as low-calcium (Class F) fly ash and the chemical composition is shown in Table 1. Analytical grade, zinc oxide (ZnO) and titanium dioxide (TiO_2) nanoparticles were supplied (particle size < 50 nm) from Sigma Aldrich [23–25].

An analytical grade 99% purity, sodium hydroxide (NaOH) was purchased from Sigma Aldrich, India. The 10 M-NaOH solution was prepared by dissolving NaOH solid in a distilled water to attain the desired concentrations. Sodium silicate solution was procured from RB scientific, Coimbatore. The alkaline solution was prepared by mixing of sodium silicate solution and 10 M sodium hydroxide solution, 24 h prior to mixing it with percussor material for sufficient gel formation.

3.3 Synthesis of hydroxyapatite from eggshell powder

The synthesis of hydroxyapatite followed the chemical precipitation method optimized for waste-derived calcium sources, as shown in Fig. 2. Cleaned and dried eggshell powder of 300 g was calcined in a muffle furnace at 900 °C for 3 h to thermally decompose calcium carbonate ($CaCO_3$) into reactive calcium oxide (CaO). After completion of calcination, the calcined powder was stored in airtight containers to avoid re-carbonation by exposure of atmospheric CO_2.

For the synthesis process, 500 mL of distilled water was poured in a 1 L borosilicate beaker and stirred magnetically. A measured volume of 220 mL of 85% phosphoric acid (H_3PO_4) was gradually added to the water under continuous stirring, allowing the mixture to cool slightly to control exothermic heat generation. The prepared CaO was then introduced in small portions to the acid solution while maintaining vigorous stirring to ensure homogeneous mixing. The pH of the reaction mixture was continuously monitored and maintained between 9 and 10 by the dropwise addition of dilute sodium hydroxide (NaOH) solution, facilitating the controlled formation of calcium phosphate. Stirring was continued for approximately 2–3 h at room temperature to promote complete precipitation [23, 24].

The final slurry was kept undisturbed for 12–24 h to confirm enough crystal nucleation and growth. Subsequently, the aged suspension was filtered using Whatman filter paper, and the obtained precipitate was washed three to four times with distilled water to remove residual ions and unreacted phosphate species. The purified hydroxyapatite precipitate was oven-dried at 100–120 °C for 6–12 h until a constant weight was achieved. The dried material was finely ground using a mortar and pestle, sieved to obtain a particle size of ≤ 50 µm, and finally stored in desiccated containers to preserve its purity prior to characterization and composite fabrication [25].

3.4 Process of pelletisation

The synthesized hydroxyapatite (HAP) powder was first converted into a compact pellet to facilitate dielectric and piezoelectric characterization as shown in Fig. 3. Approximately the required mass of HAP was weighed and placed into a hardened steel die assembly, where it was pressed using a uniaxial hydraulic press to form a cylindrical pellet. The applied compaction pressure was maintained to achieve a dense and uniform disc with a diameter of approximately 10 mm and a thickness of 2 mm, minimizing internal voids and ensuring structural integrity.

Following compaction, the green pellet was carefully removed from the die and subjected to a controlled sintering process. The specimen was placed in a muffle furnace and heated to 500 °C at a moderate heating rate to avoid thermal shock. The pellet was

Table 1 Chemical composition of flyash

Chemicals	Formula	Flyash (%)
Silicon dioxide	SiO2	62
Aluminum oxide	Al2O3	32
Iron Oxide	Fe2O3	3
Lime	CaO	0.5
Sulphur Trioxide	SO3	0.1
Magnesium Oxide	MgO	0.53
Loss of ignition	LOI	0.7

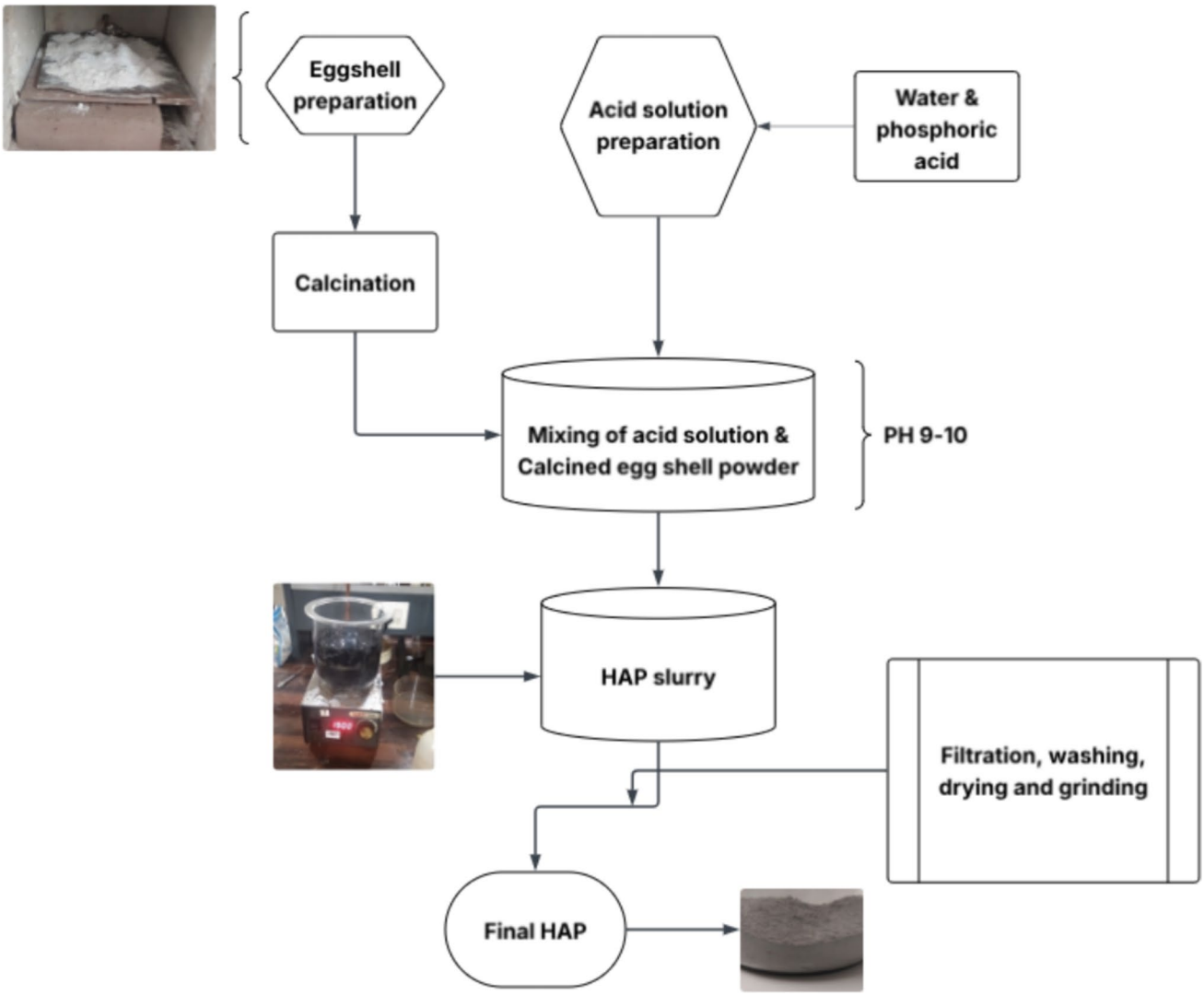

Fig. 2 Synthesis of HAP

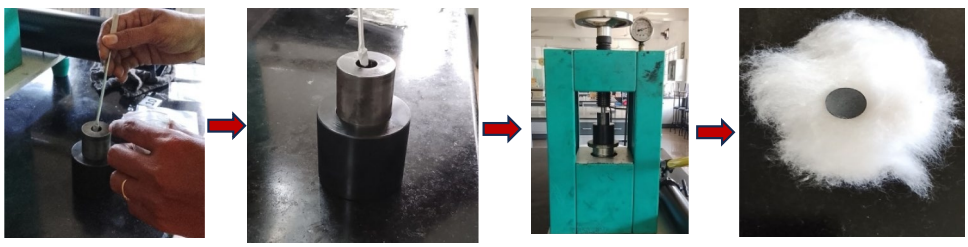

Fig. 3 The process of HAP pelletisation

held at this temperature for 2 h, allowing for partial densification, improved crystallinity, and enhanced inter-particle bonding, which are essential for reliable electrical measurements.

After sintering, the pellet was cooled gradually to room temperature inside the furnace to prevent microcracking. To prepare the specimen for dielectric and piezoelectric testing, conductive silver paste

was uniformly applied onto both flat faces of the pellet, forming stable and low-resistance electrodes. The coated pellet was then allowed to dry completely, ensuring good electrical contact for subsequent characterization tests.

3.5 Characterization of synthesized hydroxyapatite

The synthesized HAP powder was characterized to confirm its crystal structure, morphology, and dielectric properties. XRD analysis was conducted to characterize and ensure the HAP synthesis. The XRD patterns were collected in the 2θ range of 20–90° by employing Cu Kα radiation (λ = 1.5406 Å) and the related peaks were compared with the JCPDS data for hydroxyapatite [26]. The crystal size (D) was calculated applying the Scherrer Eq. (1):

$$D = \frac{K\lambda}{\beta cos\theta} \quad (1)$$

where K = 0.9 (shape factor), λ = X-ray wavelength, β = full width at half maximum, and θ = Bragg angle.

The elemental composition and Ca/P ratio were determined by means of EDS analysis, which confirmed the stoichiometric formation of hydroxyapatite (theoretical Ca/P ≈ 1.67). In order to evaluate uniformity, data were collected from several areas. Further, SEM used to examine the morphology, particle size, and structure of the synthesized powder [26]. The dielectric constant (εr) and dielectric loss tangent (tan δ) of the synthesized hydroxyapatite (HAP) were recorded within the frequency range of 1 kHz–1 MHz using an LCR meter [27].

SEM was conducted to examine the fracture morphology of the samples. Specimens were coated with a thin conductive carbon layer using a standard carbon evaporation method to prevent charging during imaging. Fractured pieces from the composite specimens were mounted on aluminum stubs using carbon adhesive tabs. Microstructural observations were performed using a Zeiss DSM-960 SEM operated under high vacuum with an accelerating voltage of 10–20 kV. Imaging was carried out mainly in secondary electron (SE) mode to observe surface topography, with BSE mode used selectively for compositional contrast. The SEM images were used to evaluate particle morphology, pore structure, and the dispersion of HAP.

3.6 Formulation of geopolymer-piezoelectric hybrid composite

The geopolymer matrix has been formulated by mixing of flyash and prepared alkaline solution. The fly ash to activator ratio was kept constant at 0.4 by weight. Along with geopolymer composite, the addition of HAP, ZnO, and TiO_2 nanoparticles was done in the proportions indicated in Table 2 to enhance piezoelectric properties.

The process of making geopolymer-piezoelectric composites is shown in Fig. 4. Using a mechanical mixer, dry components (fly ash, ZnO, TiO_2, and HAP) were initially dry blended for ten minutes to ensure the even dispersion of nanoparticles and HAP in the fly ash matrix. Sodium silicate and 12 M-NaOH solution were blended in a 2.5:1 mass ratio to prepare the alkaline activator solution separately, and the mixture was allowed to settle for 24 h prior to being used.

The dry mix was then formulated into a paste by adding the activator solution very slowly while stirring continuously. The mixture was poured into molds of 50 mm cubes and vibrate it lightly to let the air bubbles trapped inside escape. After that, the specimens were wrapped in polyethylene sheets which served to reduce moisture loss and covered with ambient conditions for 24 h and then cured in an oven at 70 °C for 48 h [28, 29]. The specimens underwent demoulding after the curing process and their surfaces are polished to eliminate the irregularities. Conductive silver wire needle electrodes were placed on the opposite sides of the cubes in order to make the voltage measurement possible during the piezoelectric testing. The samples with electrodes were kept at room temperature for 12 h for drying before the testing [28, 29].

Table 2 Mix design for hybrid geopolymer–piezoelectric composite

Component	Weight (g)	Percentage (%)	Weight ratio
Fly ash	125	50	0.50
ZnO nanoparticles	62.5	25	0.25
Eggshell-derived HAP	37.5	15	0.15
TiO_2 nanoparticles	25	10	0.10
Total	**250**	**100**	–

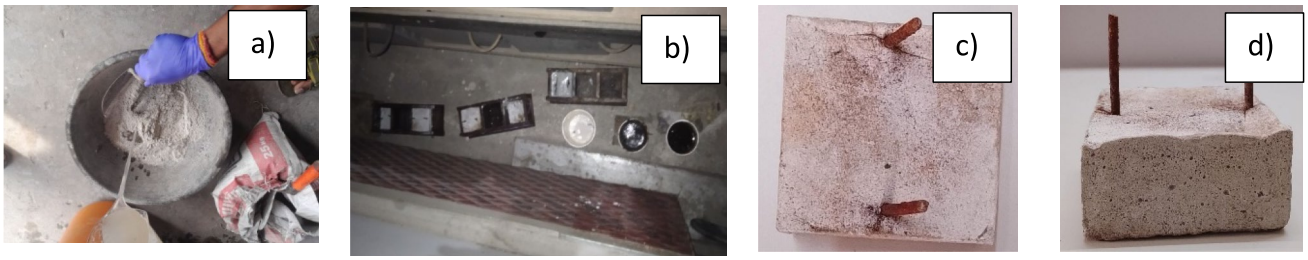

Fig. 4 The process of making geopolymer-piezo electric composites; **a** Mixing, **b** Casting, **c** & **d** Demoulded sample, respectively

3.7 Mechanical testing and electrical measurements

Compressive strength tests were performed with the help of a universal testing machine (UTM), to a maximum load of 2 mm/min. The highest load applied was noted, and compressive stress was computed taking into consideration the cross-sectional area of the specimen. The average of three specimens was taken for each mix to ensure repeatability [30, 31]. Figure 5, illustrates the test setup for the piezoelectric voltage measurements under compressive testing.

The digital multi-meter, which was configured for a 2 V range, was used to monitor the electric response of the geopolymer-piezoelectric composite during compressive loading. The electrodes that were connected to the sample were linked with the multi-meter to capture the momentary voltage output [32, 33].

4 Results and discussion

The HAP and hybrid composite were subjected to detailed characterization for determining the structural formation, dielectric performance, and electromechanical behaviour. The results from the X-ray diffraction (XRD), energy-dispersive spectroscopy (EDS), dielectric analysis, piezoelectric testing, and microstructural observation are presented and discussed in the following subsections.

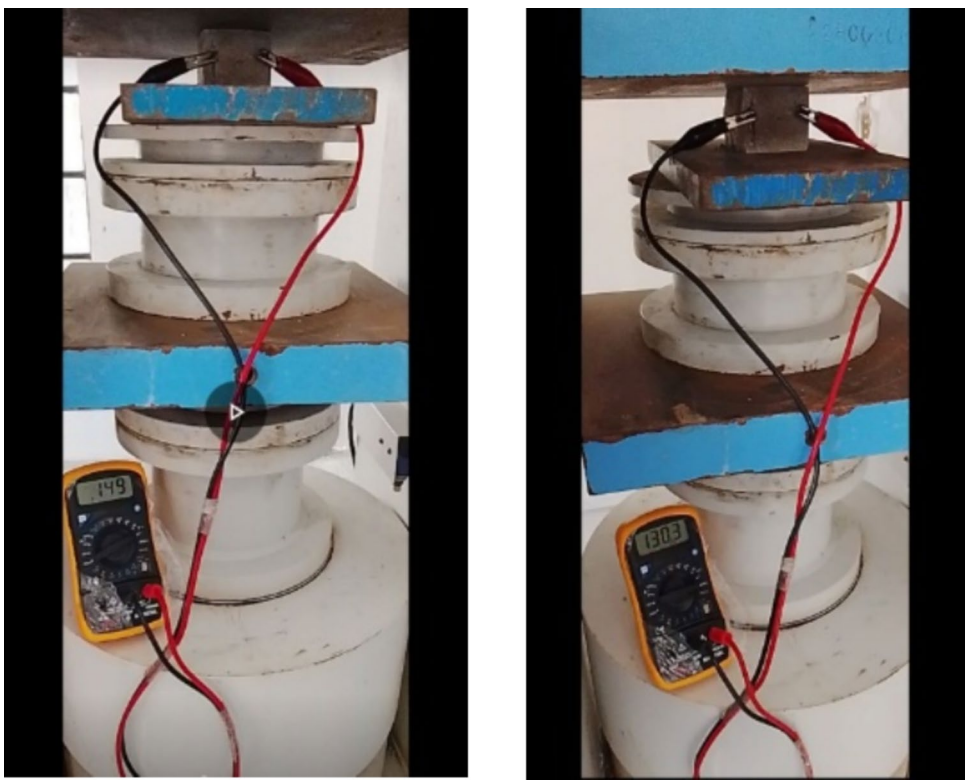

Fig. 5 Test setup of piezoelectric voltage measurement under compressive loading

4.1 Structural characterization of HAP (XRD)

The XRD pattern for the HAP showed that a crystalline calcium phosphate phase was formed as shown in Fig. 6. There were strong diffraction peaks at the angles of 2θ, which were 22.8°, 25.2°, 26.0°, 28.2°, 29.0°, 29.8°, 32.1°, and 32.5°, and they matched the hydroxyapatite planes of (200), (002), (210), (211), (112), (300), (202), and (310) respectively.

The identified peaks were in complete agreement with the standard JCPDS card No. 09–0432 thereby verifying the hexagonal crystal symmetry of the single-phase HAP. Peak sharpening was observed which is indicative of high crystallinity that is a consequence of pH control (≈9–10) and aging during the synthesis process. The average crystallite size was approximately 40–50 nm which classified the material as nanocrystalline hydroxyapatite and was calculated by the Scherrer equation on the (211) peak at 26.2°.

The absence of any secondary phases like tricalcium phosphate (TCP) and calcium oxide signifies that the precursors were almost completely converted during the synthesis process. The presence of minor peaks due to the adsorbed carbonates was so small that it could not be seen which indicates that the washing and calcination processes were effective.

Through quantitative phase analysis, it was determined that the predominant component of the synthesized powder was hydroxyapatite, while very small amounts of other substances like tribarium tellurium (VI) hexaoxide (14%), silver niobate (10%), barium nickel boride (13%) and zirconium cobalt gallide (12%) were also present, which has been shown in Table 3. The presence of these secondary phases is probably due to the addition of small amounts of elemental impurities introduced through the activator derived from fly ash or from the reaction vessel. Even though these impurities are in very small amounts, they might still be able to enhance the dielectric property together with the other mechanisms by offering additional paths for charge transport.

4.2 Dielectric properties of hydroxyapatite

The study of dielectric response is the basic characterisations, for the development of piezoelectric materials like HAP, as this phenomenon is the main factor influencing energy storage, power loss, and overall device performance. The data indicates the frequency

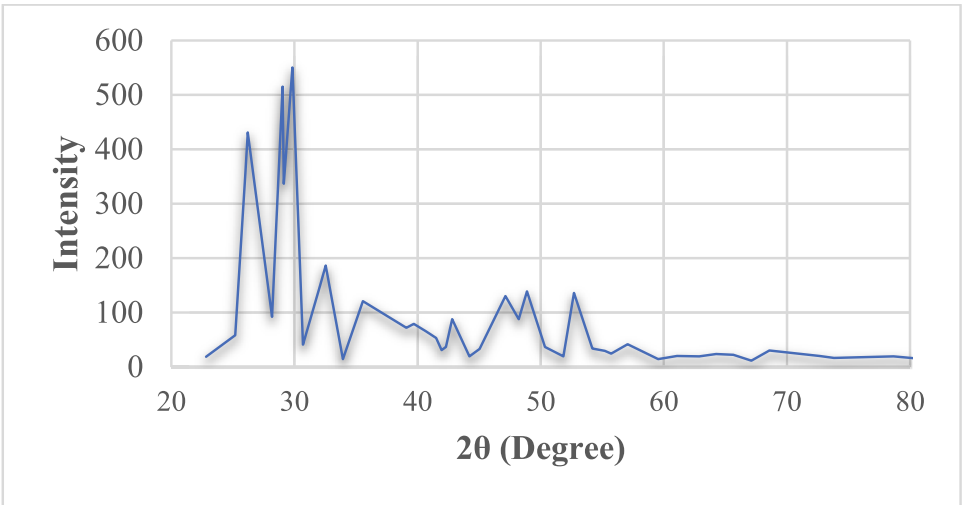

Fig. 6 XRD pattern of HAP

Table 3 Relative phase fractions identified from XRD pattern

Phase Name	Weight Fraction (%)	Possible Effect
Hydroxyapatite (HAP)	> 50	Primary piezoelectric phase
Tribarium tellurium(VI) hexaoxide	14	Dielectric stabilizer
Silver niobate	10	Charge mobility enhancer
Barium nickel boride	13	Conductive network phase
Zirconium cobalt gallide	12	Microstructural stabilizer

dependence of the HAP material's dielectric constant (ε′), which is the relative dielectric permittivity, and the dielectric loss (ε″), which relates to energy dissipation. These two parameters were examined as a function of the logarithmic frequency to discover the major polarization and relaxation mechanisms inside the material.

4.2.1 *Dielectric constant (ε′) analysis*

The behaviour of the dielectric constant (ε′) with frequency is shown in Fig. 7, and it has a characteristic dispersion profile that indicates the material ability to be polarized and its multiple phases. The highest dielectric constant, about 50,000, is reached at the low frequencies (Log f ≈ 0 Hz). This large dielectric effect is due to the charge carriers (Maxwell–Wagner-Sillars) moving and gathering at different interfaces (e.g., grain boundaries, microstructural defects, and phase boundaries). At the very low frequencies, the electric field applied is very slow that it allows the charge carriers to orient and accumulate, thus, significantly increasing the charge-storage ability of the material as a whole.

At higher frequencies, the trend is quite different, the ε′ drops off very steeply up to Log f ≈ 2 Hz. This rapid reduction signifies the relaxation of slower polarization mechanisms, particularly dipolar and interfacial polarization processes that can no longer synchronize with the faster reversal of the AC electric field. The inability of these mechanisms to trace the field oscillations results in a marked loss of polarizability and, consequently, a significant drop in the

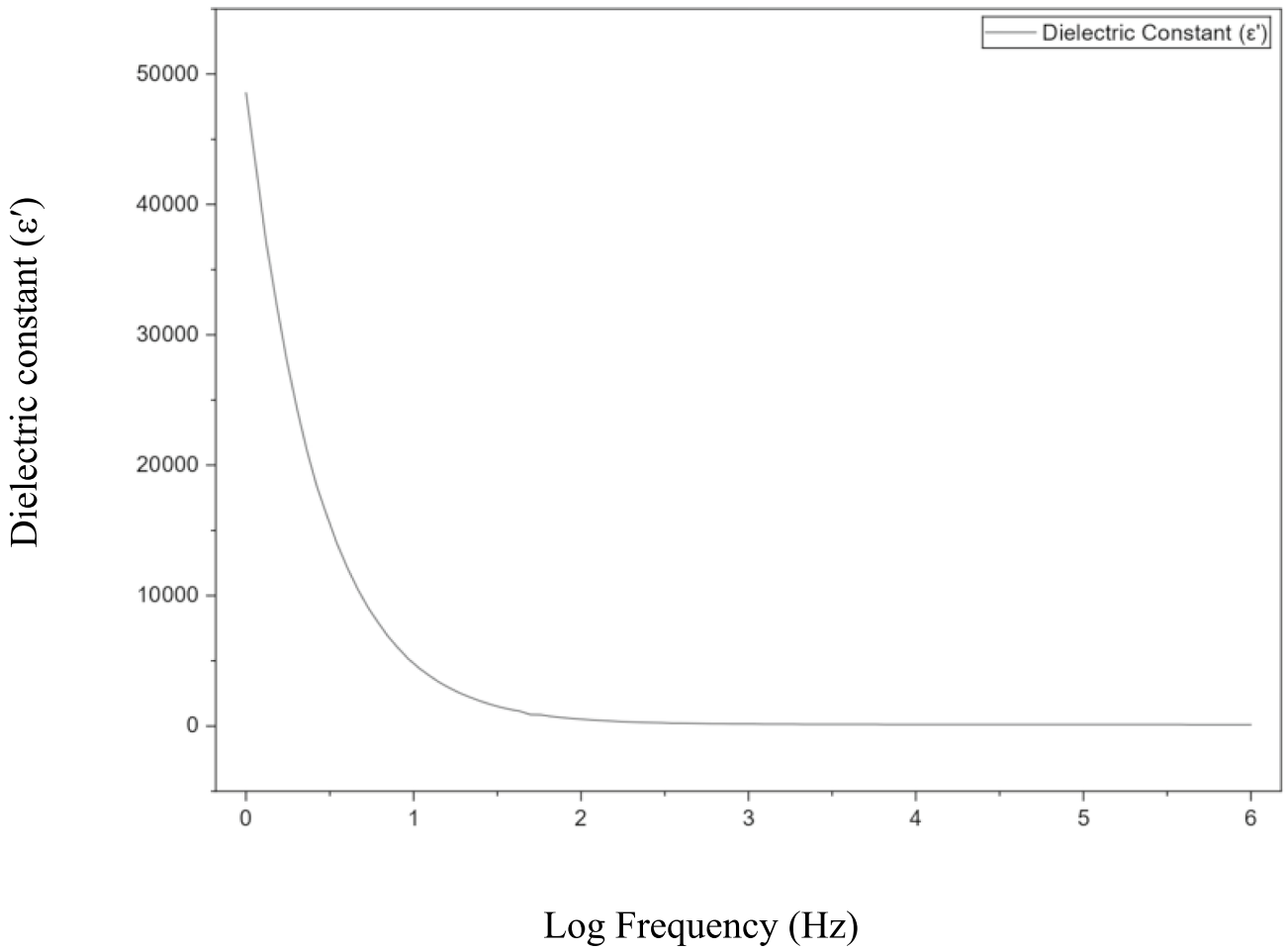

Fig. 7 Variation of dielectric constant

dielectric constant. The area links up with the polarization relaxation zone, mirroring the dynamic boundaries of the material internal charge distribution.

Outside this regime, the dielectric constant still decreases but this time the rate is much slower and more gradual and it finally stabilizes as the frequency becomes very high (Log f > 3 Hz). In this area, only electronic and atomic polarizations that have very short relaxation times can react to the rapidly oscillating field, while interfacial and dipolar components become inactive. Consequently, ε′ gets closer to a low value which is almost constant and this low value represents the inherent dielectric property of the material without any significant influence of the interfacial area[34–36].

Finally, the dielectric behaviour indicates the material outstanding low-frequency dielectric enhancement, wherein space-charge polarization constitutes the primary mechanism, yielding a clear transition to the relaxation process and finally to a high-frequency plateau being due to intrinsic polarization mechanisms. This dielectric dispersion pattern suggests a microstructure composed of different areas with various polarization modes, thus pointing out the material's suitability for the application areas where high charge-storage capability at low frequencies and stable dielectric response at high frequencies would be required.

4.2.2 Dielectric loss (ε″) analysis

Figure 8, shows the frequency-sensitive dielectric loss (ε″), which is an indicator of the materials capability to dissipate electrical energy via the processes of conduction, polarization lag, and interfacial phenomena. The dielectric loss at the lowest frequency (Log f ≈ 0 Hz) starts moderately at a value of about 8.5 which points to the occurrence of low-frequency conduction and interfacial polarization mechanisms. Simultaneously the charge carriers manage to get the time necessary to get along with the applied field, thus, there is moderate electrical dissipation.

With increasing frequency, ε″ shows an even, gradual increase, getting up to about 11.5 around Log f ≈ 1.7 for the maximum loss peak. This specific peak is associated with a dielectric relaxation process, which occurs when the electric field's angular frequency is equal to the material's relaxation time for the main dipolar or space-charge polarization process. The development of this peak suggests the presence of charge carriers or dipoles that are mobile, and the mobile dipoles are the ones that lose energy during the orientation switch. This is typical behaviour associated with Maxwell–Wagner interfacial polarization, which is widely seen in the case of heterogeneous composites or ceramics where there are different conductivities across microstructural interfaces[37, 38].

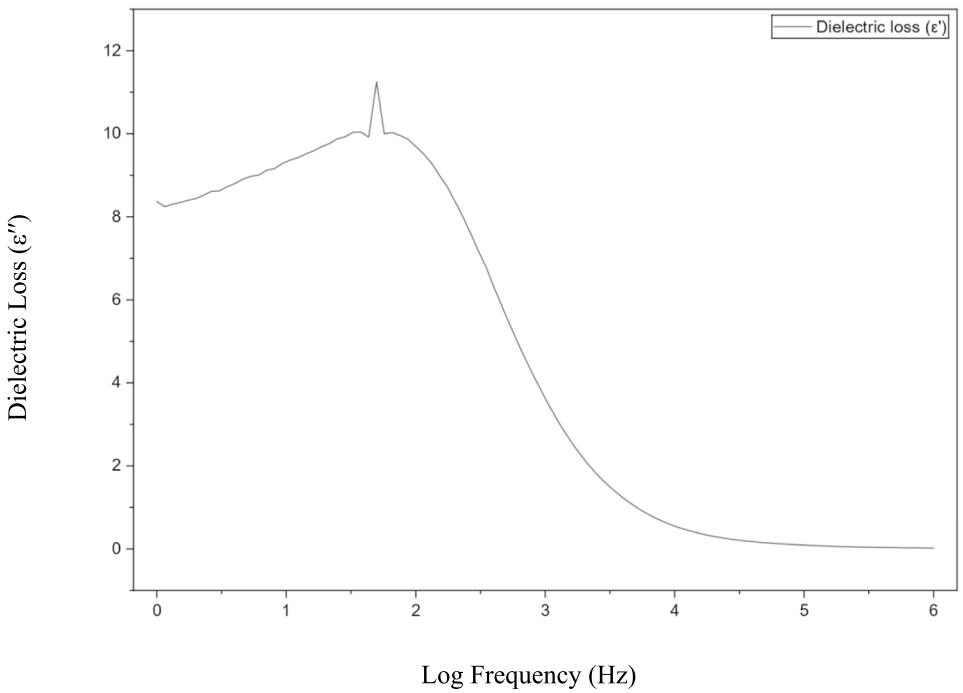

Fig. 8 Loss tangent as a function of frequency

The dielectric loss reveals a steep decline, beyond the relaxation frequency, which means that the polarization process that caused the peak is no longer able to follow the field's fast variations. The slow-moving charges and dipoles cannot reorient at these higher frequencies; hence their contribution is insignificant. As a result, the dielectric loss drops quickly and finally comes down very close to zero as the frequency surpasses Log f > 4 Hz. The almost disappearing ε″ in this range of high-frequency implies an extremely low-energy dissipation, thus confirming that only fast polarization mechanisms, mainly electronic polarization, are in action.

The principal dielectric loss pattern reveals the occurrence of a distinctly relaxation process and the material being highly effective at high frequencies, where the energy loss becomes trivial. Its such feature is a plus for applications that need low-loss dielectric materials, for instance, high-frequency capacitors, insulation parts, and power-saving electronic materials.

4.3 Microstructural observation of HAP

To understand the characteristics of particle shape, grain connectivity, and porosity, the surface morphology of the synthesized HAP from eggshell powder was studied with the help of scanning electron microscopy. Representative SEM micrographs at 2 μm and 1 μm scale bars are shown in Fig. 9a and b, respectively, which were taken at corresponding magnifications.

The lower magnification micrograph (Fig. 9a) shows that the HAP powder is made up of mainly irregularly shaped agglomerates which consist of fine primary particles. These agglomerates have an open structure and are not fully dried because of the low-temperature drying process, the same process that gives them their sponge-like appearance. Such open spaces can allow the activator solution to penetrate during the composite manufacturing process, thereby resulting in a stronger mechanical bond with the geopolymer matrix through interlocking. The particle size distribution is from sub-micron to a few microns, with the clusters being held together loosely by forces on the surface, a morphological characteristic of chemically precipitated hydroxyapatite.

Upon the application of higher magnification (Fig. 9b), the primary HAP grains exhibit a morphology that is nearly spherical to somewhat rod-like and have an average diameter ranging from 80 to 300 nm. The particles have smooth surfaces and distinct grain boundaries, signifying a high level of crystallinity, in agreement with the XRD findings. Nanoscale pores and voids between the particles are seen which indicates that the material synthesized has a large specific surface area that is advantageous for the dielectric polarization enhancement in the composite system.

There is no visible contamination, secondary crystalline inclusions, and amorphous residues, thereby proving the chemical purity and uniformity of the synthesis route. The nanoscale roughness and even grain distribution suggest that the precipitation process produced HAP crystals with good nucleation and very

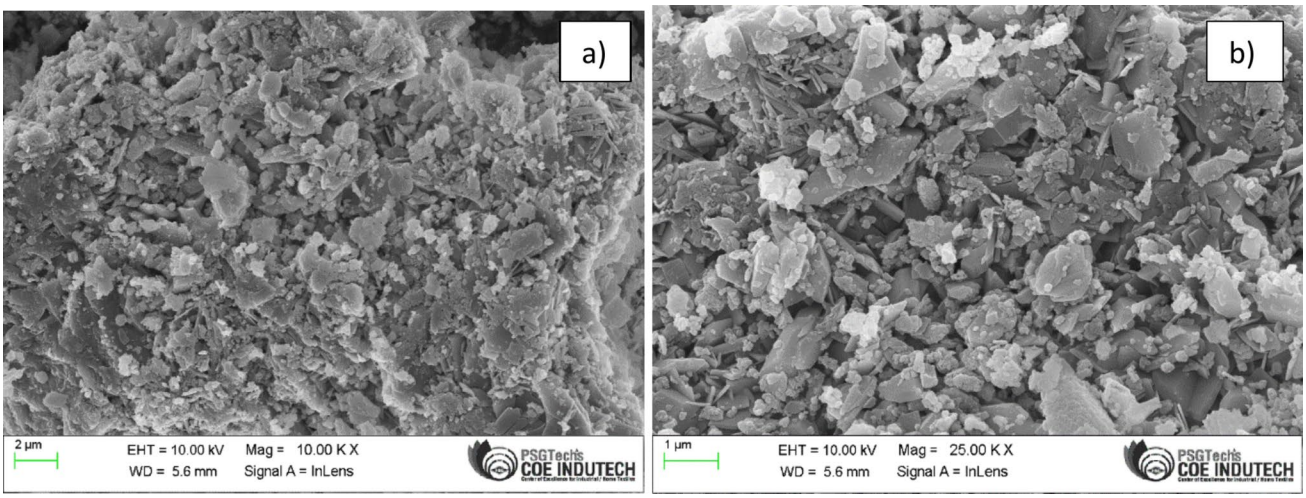

Fig. 9 SEM images of fractured surface of hybrid geopolymer–HAP composite showing uniform dispersion and dense matrix

little growth coalescence. The mentioned microstructural features are favourable for the upcoming incorporation into the geopolymer binder as they could provide the necessary intimate particle contact and reactive surface sites for strong interfacial bonding.

Finally, SEM analyses confirm that the process of converting eggshell to HAP is effective, as it yields fine, porous, and uniformly distributed nanocrystals. Such morphological characteristics are directly responsible for the better dielectric performance since they help charge to build up at the interfaces of grains and also help to transfer the stress during mechanical loading.

4.4 Piezoelectric response under compressive loading, measured electrical output

An observable piezoelectric voltage output was produced by the hybrid geopolymer composite when compressive stress was applied to it. The highest voltage instantly recorded was 0.149 V at a pressure of 22.12 MPa. The stress applied caused an increase in the produced voltage that was almost linear within the elastic range, as shown in Fig. 10.

The outcome demonstrates the composite's capacity to transform mechanical energy into electrical energy, thus proving the successful insertion of polar phases (HAP, ZnO, TiO_2) into the geopolymer matrix. In spite of the small amount compared to that of commercial PZT ceramics, it is still considered as a remarkable performance for a lead-free, low-temperature processed system.

This study analysed that the addition of HAP up to 15 wt% gave the best increase in dielectric and piezoelectric properties. At the lower concentrations, the number of polarization centers was not enough to produce the expected voltage, while at the higher concentrations there was a chance of particle agglomeration which would lead to loss of mechanical integrity. Therefore, the composition of 15% HAP was chosen as it provides a good combination of functional performance and structural stability [39, 40].

Further, the direct piezoelectric response of ZnO comes from its wurtzite structure, but TiO_2 (anatase) increases surface charge trapping and the dielectric constant. The presence of both materials together allows for increased voltage generation by facilitating the movement of electrons between the conductive interfaces. Furthermore, the two oxides help to improve the microstructure by providing nucleation

Fig. 10 Voltage output of geopolymer and HAP composite

sites for the formation of geopolymer gel during the process [41–43].

In addition, the interactions that happen at the atomic level between calcium ions released from HAP with silanol/aluminosilicate groups in the geopolymer matrix to form bonds that are quite strong at the interface. This makes it possible for the forces to be effectively transferred during compressive loading and also causes less energy to be lost in the process. Surface interaction of this kind is very important for

consistent piezoelectric performance and durability over a long period of time [44, 45].

The hybrid composite's compressive strength was found to be 22.12 MPa, which indicates that the addition of functional filler did not affect the mechanical performance of the composite as much as the case of conventional geopolymers with similar composition. The strength can be used for non-structural and light-load-bearing applications. The small reduction in compressive strength that can be observed in the hybrid composite with respect to pure geopolymer reference samples can be explained by the presence of rigid particles which hinder gel formation. Nevertheless, the trade-off is compensated by the additional electrical functionality.

5 Potential applications and limitations

The developed hybrid geopolymer, hydroxyapatite composite offers significant potential for smart and sustainable construction applications. Its ability to convert mechanical stress into electrical output enables use in self-sensing components, energy-harvesting pavements, and façade or flooring systems where electromechanical responsiveness enhances performance. The low-temperature synthesis and reliance on waste-derived resources make the material particularly suitable for environmentally conscious infrastructure projects. However, certain limitations must be addressed before large-scale implementation. The generated voltage, while measurable, remains relatively low compared with conventional piezoelectric ceramics, necessitating optimization of phase dispersion, poling, and interfacial bonding. Additionally, long-term durability under cyclic loading and variable environmental conditions requires further evaluation. Despite these challenges, the material's scalability, low embodied energy, and compatibility with standard cementitious processing position it as a promising candidate for next-generation, self-powered sensing elements in sustainable construction systems.

6 Conclusions

The research ensures the sustainable and operational way for developing piezoelectric geopolymer composites from the hydroxyapatite prepared from waste eggshell powder. The key features of the study includes eggshell waste has been turned into high-purity hydroxyapatite using a controlled wet-chemical precipitation method at room temperature. XRD confirmed the presence of crystalline HAP with hexagonal symmetry and an average crystallite size of about 45 nm. EDS analysis gave a Ca/P ratio of 1.66, which is in line with stoichiometric hydroxyapatite. The addition of 15 wt % HAP, along with ZnO (25%) and TiO_2 (10%) nanoparticles, to the fly ash geopolymer matrix resulted in a composite that was dense and homogeneous. Further, the hybrid composite generated a voltage output of 0.149 V under 22.12 MPa compressive stress, demonstrating effective electromechanical coupling. The synergistic interaction between HAP, ZnO, and TiO_2 contributed to improved charge polarization and dielectric stability. The compressive strength of the modified geopolymer stayed at approximately 22 MPa, adequate for non-heavily structural uses, hence electricity function was gained without substantial trade-off in the load-bearing ability.

The research ensures that development of eco-friendly piezoelectric geopolymer composites is feasible by utilizing hydroxyapatite from eggshells in combination with fly ash. The method paves the way for environmentally friendly and low-temperature thermal smart building materials. Composites are primarily recommended for non-structural applications like façade panels, tiles, and pavements, where electromechanical responsiveness can be a significant functional added value. Overall, the present framework, is technically sound and sustainable for the use of waste-derived, energy-responsive geopolymer composites in smart infrastructure.

Acknowledgements

The authors thank the Department of Civil Engineering, PSG Sons' and Charities for their support.

Author Contributions

Arun Murugesan: Conceptualization; Methodology; Experimental work; Data curation; Formal analysis; Writing – original draft preparation. Nidhya Rathinavel: Material preparation; Laboratory investigations; Critical review and editing; Visualization; Data interpretation; Writing – review and editing. Karthick Jaisankar: Hydroxyapatite synthesis; Characterization

studies (XRD, SEM, EDS); Validation; Draft editing. Balaji Ravi: Geopolymer formulation; Mechanical testing; Resources; Supervision of laboratory procedures. Natrayan Lakshmaiya: Conceptualization; Supervision; Project administration; Interpretation of results; Final approval of the manuscript. All authors have read and approved the final manuscript.

Funding

Authors declared that no funding was received for this Research and Publication.

Data availability

All data supporting the findings of this study are available from the corresponding author upon reasonable request.

Declarations

Competing Interest The authors declare no competing interests.

Ethical approval This study did not involve human participants or animal testing. All experimental procedures complied with institutional environmental and safety regulations.

References

1. B.D. Olagunju, O.A. Olanrewaju, Life cycle assessment of ordinary portland cement (OPC) using both problem oriented (Midpoint) approach and damage oriented approach (Endpoint). Product Life Cycle-Opport. Digital Sust. Transf. (2021). https://doi.org/10.5772/intechopen.98398
2. N. Marandi, S. Shirzad, Sustainable cement and concrete technologies: A review of materials and processes for carbon reduction. Innov. Infrastruct. Solut. **10**, 408 (2025)
3. Z. He, X. Zhu, J. Wang, M. Mu, Y. Wang, Comparison of CO2 emissions from OPC and recycled cement production. Constr. Build. Mater. **211**, 965–973 (2019)
4. N. Shehata, O.A. Mohamed, E.T. Sayed, M.A. Abdelkareem, A.G. Olabi, Geopolymer concrete as green building materials: recent applications, sustainable development and circular economy potentials. Sci. Total. Environ. **836**, 155577 (2022)
5. A.G. Olabi, N. Shehata, U.H. Issa, O.A. Mohamed, M. Mahmoud, M.A. Abdelkareem, M.A. Abdelzaher, The role of green buildings in achieving the sustainable development goals. Int. J. Thermofluids **25**, 101002 (2025)
6. O.A. Mohamed, A. Hassan, N.R. Abdelwahab, High-performance and durable green geopolymer based on slag/alumina sludge ash incorporating $CuFe_2O_4$ Spinel nanograins for enhanced gamma radiation shielding. Int. J. Concr. Struct. Mater. **19**, 87 (2025)
7. B.B. Jindal, T. Alomayri, A. Hasan, C.R. Kaze, Geopolymer concrete with metakaolin for sustainability: a comprehensive review on raw material's properties, synthesis, performance, and potential application. Environ. Sci. Pollut. Res. **30**, 25299–25324 (2023)
8. G. Lamaa, D. Suescum-Morales, A.P.C. Duarte, R.V. Silva, J. de Brito, Optimising the performance of CO2-cured alkali-activated aluminosilicate industrial by-products as precursors. Materials (Basel). **16**, 1923 (2023)
9. K. Fernando, Investigation of rice husk ash as a sustainable source material for blended low calcium fly ash based alkali activated binders, (2024).
10. S.G.K.M. Kumar, J.M. Kinuthia, J. Oti, B.O. Adeleke, Geopolymer chemistry and composition: a comprehensive review of synthesis, reaction mechanisms, and material properties—oriented with sustainable construction. Materials (Basel). **18**, 3823 (2025)
11. X. Cao, Y. Xiong, J. Sun, X. Zhu, Q. Sun, Z.L. Wang, Piezoelectric nanogenerators derived self-powered sensors for multifunctional applications and artificial intelligence. Adv. Funct. Mater. **31**, 2102983 (2021)
12. T. Vijayakanth, S. Shankar, G. Finkelstein-Zuta, S. Rencus-Lazar, S. Gilead, E. Gazit, Perspectives on recent advancements in energy harvesting, sensing and bio-medical applications of piezoelectric gels. Chem. Soc. Rev. **52**, 6191–6220 (2023)
13. D. Pan, Lead zirconate titanate (PZT) piezoelectric ceramics: applications and prospects in human motion monitoring. Ceram.-Silik. **68**, 444–458 (2024)
14. R. Prasad, Development and Characterisation of Lead-Free Smart Cement Composites for Structural Health Monitoring System, (2022).
15. A. Aabid, B. Parveez, M.A. Raheman, Y.E. Ibrahim, A. Anjum, M. Hrairi, N. Parveen, J. Mohammed Zayan, A review of piezoelectric material-based structural control and health monitoring techniques for engineering structures: Challenges and opportunities, in: Actuators, MDPI, (2021): p. 101.

16. V. Saxena, I. Shukla, L.M. Pandey, Hydroxyapatite: an inorganic ceramic for biomedical applications, in *Mater. Biomed. Eng.* (Elsevier, 2019), pp.205–249
17. A.K. Sánchez-Hernández, R. Lozano-Rosas, J.J. Gervacio-Arciniega, J. Wang, M.J. Robles-Águila, Piezoelectric and mechanical properties of hydroxyapatite/titanium oxide composites. Ceram. Int. **48**, 23096–23103 (2022)
18. A.A. Bayoumi, S.M.A. El-Gamal, M.H. Khedr, W.M.A. El Rouby, O.A. Mohamed, Promoting the mechanical features and thermal endurance of OPC-pumice composites using functionalized multi-walled carbon nanotubes grafted with nano-silica. Innov. Infrastruct. Solut. **10**, 550 (2025)
19. O.A. Mohamed, M.M. Hazem, A. Mohsen, M. Ramadan, Impact of microporous γ-Al_2O_3 on the thermal stability of pre-cast cementitious composite containing glass waste. Constr. Build. Mater. **378**, 131186 (2023)
20. A.M. Rashad, A.K. Eessaa, M.H. Khalil, O.A. Mohamed, An initial study on the effect of nano-zirconium on the behavious of alkali-activated slag cement subjected to sea-water attack. Constr. Build. Mater. **370**, 130659 (2023)
21. M.S. Amin, M. Heikal, H.H. Negm, A.M. Abu-Dief, O.A. Mohamed, Manufacture of eco-friendly cementitious building materials of high performance from Egyptian industrial solid wastes. Constr. Build. Mater. **406**, 133446 (2023)
22. H. Mamdouh, A. Hassan, N. Zenhom, A. Ali, O.A. Mohamed, A. Salman, Splicing behaviour of GFRP, BFRP, and steel bars in reinforced concrete beams. Discov. Appl. Sci. **7**, 1–27 (2025)
23. D.L. Goloshchapov, V.M. Kashkarov, N.A. Rumyantseva, P.V. Seredin, A.S. Lenshin, B.L. Agapov, E.P. Domashevskaya, Synthesis of nanocrystalline hydroxyapatite by precipitation using hen's eggshell. Ceram. Int. **39**, 4539–4549 (2013)
24. Y. Wang, C. He, G. Li, X. Liu, L. Liu, Y. Jiao, Sustainable Ca (OH) 2 deacidifiers derived from waste eggshells for free fatty acids removal: characterization, performance and thermodynamicsEnviron. Dev. Sustain. (2025). https://doi.org/10.1007/s10668-025-06363-5
25. F. Hamidivadigh, J. Javadpour, The synthesis of hydroxyapatite nanoparticles using eggshells and two different phosphate sources. Eur. J. Eng. Technol. Res. **9**, 1–4 (2024)
26. N.A.S.M. Pu'ad, J. Alipal, H.Z. Abdullah, M.I. Idris, T.C. Lee, Synthesis of eggshell derived hydroxyapatite via chemical precipitation and calcination method. Mater. Today Proc. **42**, 172–177 (2021)
27. P.H. Bolivar, M. Brucherseifer, J.G. Rivas, R. Gonzalo, I. Ederra, A.L. Reynolds, M. Holker, P. De Maagt, Measurement of the dielectric constant and loss tangent of high dielectric-constant materials at terahertz frequencies. IEEE Trans. Microw. Theory Tech. **51**, 1062–1066 (2003)
28. H. Chkala, I. Kirm, S. Ighir, A. Ourmiche, M. Chigr, N.-E. El Mansouri, Preparation and characterization of eco-friendly composite based on geopolymer and reinforced with date palm fiber. Arab. J. Chem. **17**, 105510 (2024)
29. R.S. Raj, G.P. Arulraj, N. Anand, B. Kanagaraj, E. Lubloy, M.Z. Naser, Nanomaterials in geopolymer composites: A review. Dev. Built Environ. **13**, 100114 (2023)
30. S. Nagajothi, S. Elavenil, S. Angalaeswari, L. Natrayan, W.D. Mammo, Durability studies on fly ash based geopolymer concrete incorporated with slag and alkali solutions. Adv. Civ. Eng. **2022**(1), 7196446 (2022)
31. M.N. Amin, K. Khan, W. Ahmad, M.F. Javed, H.J. Qureshi, M.U. Saleem, M.G. Qadir, M.I. Faraz, Compressive strength estimation of geopolymer composites through novel computational approaches. Polymers (Basel) **14**, 2128 (2022)
32. S. Mondal, T. Mukhopadhyay, F. Scarpa, S. Naskar, Frequency-band programmable piezoelectric energy harvesters with variable substrate material, tip mass and fractal architectures: Experimental and numerical investigations. Mech. Based Des. Struct. Mach. **53**, 1603–1634 (2025)
33. N.A.K.Z. Abidin, N.M. Nayan, M.M. Azizan, A. Ali, N. Hussin, N.A. Azli, N.M. Nordin, The simulation analysis of piezoelectric transducer with multi-array configuration. J. Phys. Conf. Ser. **1432**, 012042 (2020)
34. V.S. Nadh, C. Krishna, K. Kumar, K.S. Nitesh, G.B. Raja, P. Paramasivam, Structural behavior of nanocoated oil palm shell as coarse aggregate in lightweight concrete. J. Nanomater. **2021**(1), 4741296 (2021)
35. M.M. Hassan, W. Khan, A. Azam, A.H. Naqvi, Influence of Cr incorporation on structural, dielectric and optical properties of ZnO nanoparticles. J. Ind. Eng. Chem. **21**, 283–291 (2015)
36. X. Cheng, G. Ye, H. Sun, T. Li, C. Sun, Analysis of low-frequency dielectric loss of XLPE cable insulation based on extended Debye model. AIP Adv. **11**, 085103 (2021)
37. T. Tian, D. Scullion, D. Hughes, L.H. Li, C.-J. Shih, J. Coleman, M. Chhowalla, E.J.G. Santos, Electronic polarizability as the fundamental variable in the dielectric properties of two-dimensional materials. Nano Lett. **20**, 841–851 (2019)
38. M. Senthil Kumar, R.D. Hemanth, K. Annamalai, E. Karthick, Experimental investigations on mechanical and microstructural properties of Al2O3/SiC reinforced hybrid metal matrix composite. Mater. Sci. Eng. **402**, 012123 (2018)
39. R. Rodriguez, D. Rangel, G. Fonseca, M. Gonzalez, S. Vargas, Piezoelectric properties of synthetic

hydroxyapatite-based organic-inorganic hydrated materials. Results Phys. **6**, 925–932 (2016)
40. R. Rodriguez, M. Estevez, S. Vargas, R. Salazar, F. Pacheco, Hap-based porous material with potential application as bio-packages for MEMS. J. Mater. Sci. Mater. Electron. **19**, 646–652 (2008)
41. R. Ben Belgacem, M. Chaari, A. Matoussi, Studies on structural and electrical properties of ZnO/TiO2 composite materials. J. Alloys Compd. **651**, 49–58 (2015)
42. S. Lin, L. Songyuan, F. Yaochong, Facile preparation of ZnO/TiO 2 nanocomposite photocatalysts and study of their photocatalytic performance. J. Ovonic Res. (2023). https://doi.org/10.15251/jor.2023.196.739
43. M. Chen, Z. Kang, J. Wu, N. Qin, D. Bao, Significantly enhanced piezo-photocatalytic properties of recyclable nanocomposite films by growing ZnO nanorods on inverse opal structured TiO2 framework. J. Alloys Compd. **985**, 174032 (2024)
44. W. Huo, Z. Zhu, S. Pu, R.Y.M. Li, Interfacial properties and interaction of calcium-based geopolymer gels-SiO2 aggregate based on molecular dynamics simulations. J. Non-Cryst. Solids **665**, 123607 (2025)
45. B. Ma, Y. Luo, L. Zhou, Z. Shao, R. Liang, J. Fu, J. Wang, J. Zang, Y. Hu, L. Wang, The influence of calcium hydroxide on the performance of MK-based geopolymer. Constr. Build. Mater. **329**, 127224 (2022)